Solid Earth, 8, 361–378, 2017
www.solid-earth.net/8/361/2017/
doi:10.5194/se-8-361-2017

Solid Earth
Open Access

Precise age for the Permian–Triassic boundary in South China from high-precision U-Pb geochronology and Bayesian age–depth modeling

Björn Baresel[1], Hugo Bucher[2], Morgane Brosse[2], Fabrice Cordey[3], Kuang Guodun[4], and Urs Schaltegger[1]

[1]Department of Earth Sciences, University of Geneva, Geneva, 1205, Switzerland
[2]Paleontological Institute and Museum, University of Zurich, Zurich, 8006, Switzerland
[3]Laboratoire de Géologie de Lyon, CNRS-UMR 5265, Université Claude Bernard Lyon 1, Villeurbanne, 69622, France
[4]Guangxi Bureau of Geology and Mineral Resources, Nanning, 530023, China

Correspondence to: Björn Baresel (bjoern@heldenepos.de)

Received: 17 October 2016 – Discussion started: 28 October 2016
Revised: 13 February 2017 – Accepted: 27 February 2017 – Published: 30 March 2017

Abstract. This study is based on zircon U-Pb ages of 12 volcanic ash layers and volcanogenic sandstones from two deep water sections with conformable and continuous formational Permian–Triassic boundaries (PTBs) in the Nanpanjiang Basin (South China). Our dates of single, thermally annealed and chemically abraded zircons bracket the PTB in Dongpan and Penglaitan and provide the basis for a first proof-of-concept study utilizing a Bayesian chronology model comparing the three sections of Dongpan, Penglaitan and the Global Stratotype Section and Point (GSSP) at Meishan. Our Bayesian modeling demonstrates that the formational boundaries in Dongpan (251.939 ± 0.030 Ma), Penglaitan (251.984 ± 0.031 Ma) and Meishan (251.956 ± 0.035 Ma) are synchronous within analytical uncertainty of ~ 40 ka. It also provides quantitative evidence that the ages of the paleontologically defined boundaries, based on conodont unitary association zones in Meishan and on macrofaunas in Dongpan, are identical and coincide with the age of the formational boundaries. The age model also confirms the extreme condensation around the PTB in Meishan, which distorts the projection of any stratigraphic points or intervals onto other more expanded sections by means of Bayesian age–depth models. Dongpan and Penglaitan possess significantly higher sediment accumulation rates and thus offer a greater potential for high-resolution studies of environmental proxies and correlations around the PTB than Meishan. This study highlights the power of high-resolution radio-isotopic ages that allow a robust intercalibration of patterns of biotic changes and fluctuating environmental proxies and will help recognizing their global, regional or local significance.

1 Introduction

The Permian–Triassic boundary mass extinction (PTBME) is considered the largest mass extinction within the Phanerozoic. About 90 % of all marine species suffered extinction (Raup, 1979; Stanley and Yang, 1994; Erwin et al., 2002; Alroy et al., 2008) and terrestrial plant communities underwent major ecological reorganization (Hochuli et al., 2010). This major caesura in global biodiversity marked the end of the Palaeozoic faunas and the inception of the modern marine and terrestrial ecosystems (e.g., Benton, 2010; Van Valen, 1984). Several kill mechanisms have been proposed, such as global regression (e.g., Erwin 1990; Yin et al., 2014), marine anoxia (e.g., Feng and Algeo, 2014), ocean acidification (e.g., Payne et al., 2010) or a combination thereof. Rapid global warming (e.g., Svensen et al., 2009), high nutrient fluxes from continent into oceans (Winguth and Winguth, 2012) and increased sediment accumulation rates (Algeo and Twitchett, 2010) also came into the play, but their respective relations with the global regression near the PTB and the main extinction peak at the PTB remain unclear. In spite of the rapidly growing amount of data, the detailed timing of available diversity estimates and environmental proxies is still lacking, and the ultimate triggers of the PTBME re-

Published by Copernicus Publications on behalf of the European Geosciences Union.

main elusive. The most likely cause derives from the temporal coincidence with massive and short-lived volcanism of the Siberian Traps (e.g., Burgess and Bowring, 2015) that injected excessive amounts of volatiles (H_2O, CO_2, SO_2, H_2S) into the atmosphere. Accompanying destabilization of gas hydrates (CH_4) and contact metamorphism of organic carbon-rich sediments (Retallack and Jahren, 2008; Svensen et al., 2009) are likely to have contributed additional volatiles into the atmosphere, thus substantially altering the climate and the chemical composition of the ocean. This presumably close chronological association has led many authors to support a cause–effect relationship between flood basalt volcanism and mass extinctions. Constraining the timing and duration of the PTBME in a precisely and accurately quantified model that combines relative (i.e., biostratigraphy, environmental changes) and sequences of absolute (zircon geochronology) ages is key to reveal the cascading causes and effects connecting rapid environmental perturbations to biological responses.

The South China block provides a few exceptional marine successions with a continuous stratigraphic record across the PTB (e.g., Yin et al., 2014). Among these is the Global Stratotype Section and Point (GSSP) in Meishan D (Yin et al., 2001), where the PTB is defined by the first occurrence (FO) of the Triassic conodont *Hindeodus parvus*. Additionally, these South Chinese sections reflect intense regional volcanic activity during late Permian and Early Triassic times as manifested by many intercalated zircon-bearing ash beds (Burgess et al., 2014; Galfetti et al., 2007; Lehrmann et al., 2015; Shen et al., 2011). High-precision U-Pb zircon geochronology can be applied to these ash beds by assuming that the age of zircon crystallization closely approximates the age of the volcanic eruption and ash deposition. Earliest U-Pb geochronological studies (e.g., Bowring et al., 1998; Mundil et al., 2004; Ovtcharova et al., 2006; Shen et al., 2011) do not reach decamillennial resolution, which is necessary to resolve biotic events, such as extinction or recovery. Recent improvements in the U-Pb dating technique by the development of the chemical abrasion–isotope dilution–thermal ionization mass spectrometry (CA-ID-TIMS; Mattinson, 2005), by the revision of the natural U isotopic composition (Hiess et al., 2012), by the development of data reduction software (Bowring et al., 2011; McLean et al., 2011) and by the calibration of the EARTHTIME ^{202}Pb-^{205}Pb-^{233}U-^{235}U tracer solution (Condon et al., 2015) now provide more accurate weighted mean zircon population dates at the <80 ka level (external uncertainty) for a PTB age, which allow for more precise calibration between biotic and geologic events during mass extinctions and recoveries. Two of the cases benefiting from this improved technique are the highly condensed GSSP defining the PTB at Meishan (Burgess et al., 2014) and the expanded Early–Middle Triassic boundary in Monggan (Ovtcharova et al., 2015).

The aim of this work is (1) to date the PTB in two sedimentary sections that are continuous with a conformable PTB and with higher sediment accumulation rates over the same duration than in Meishan, using the highly precise and accurate dating technique of CA-ID-TIMS, and (2) to test the age consistency between the PTB as defined paleontologically in Meishan and as recognized by conformable formational boundaries in the deeper water sections of Dongpan and Penglaitan. Our high-precision dates provide a future test for the synchronicity of conodont biozones, chemostratigraphic correlations, and other proxies involved in the study of the PTBME. Moreover, applying Bayesian age modeling (Haslett and Parnell, 2008) based on these high-precision data sets allows us to model variations in sediment accumulation rate and to directly compare other proxy data across different PTB sections, inclusive of the Meishan GSSP.

Our data demonstrate that the PTB, as recognized in our sections by conformable boundaries between late Permian and basal Triassic formations, is synchronous within analytical uncertainty of ca. 40 ka. We also show that Bayesian age models produce reproducible results from different sections, even though U-Pb datasets originate from different laboratories. We construct a coherent age model for the PTB in Dongpan and Penglaitan, which is also in agreement with the PTB age model from Meishan (Burgess et al., 2014). These results further demonstrate that ^{206}Pb / ^{238}U dates produced in two different laboratories using the EARTHTIME tracer solution provide reproducible age information at the 0.05 % level of uncertainty.

2 Geological setting

2.1 Regional context

The newly investigated volcanic ash beds were sampled from two PTB sections: Dongpan in southwestern Guangxi Province and Penglaitan in central Guangxi Province in South China (Fig. 1a, exact sample locations are given in Sect. S1 in the Supplement). Both sections are within the Nanpanjiang Basin (Lehrmann et al., 2015), a late Permian–Early Triassic pull-apart basin in a back arc context located on the present-day southern edge of the South China block. This deep-marine embayment occupied an equatorial position in the eastern paleo-Tethys Ocean (e.g., Golonka and Ford, 2000; Lehrmann et al., 2003; Fig. 1b). The basin was dominated by a mixed carbonate–siliciclastic regime during Permian and Early Triassic times and underwent a major change to a flysch-dominated regime in later Triassic times (e.g., Galfetti et al., 2008; Lehrmann et al., 2007). Decimeter- to meter-thick beds of mixed volcanic and clastic material as well as millimeter- to centimeter-thick volcanic ash beds are locally abundant and especially well preserved in down-thrown blocks recording deep water records in low energy environments and, to a lesser degree, on up-thrown blocks recording shallow water to outer platform settings. Volcanic ash beds are, however, usually not preserved in traction-

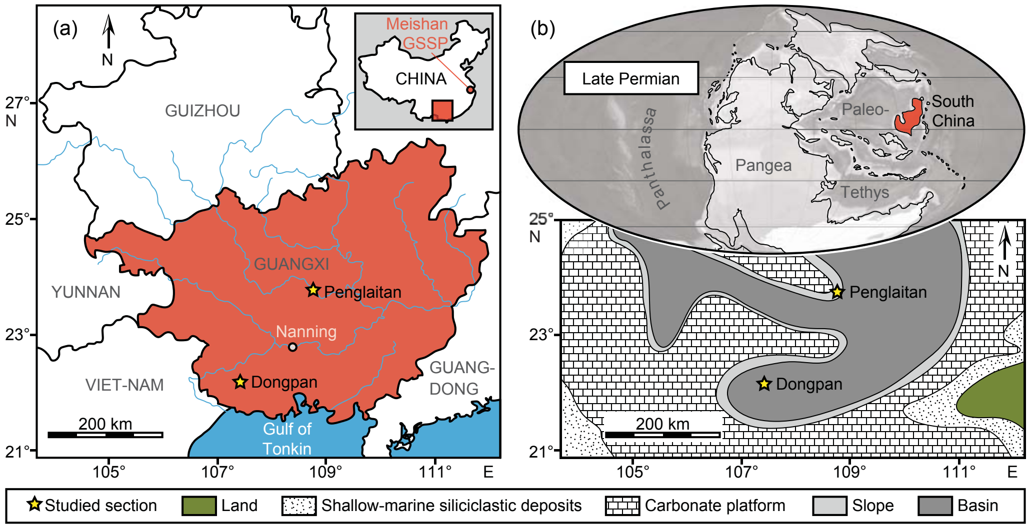

Figure 1. (a) Locality map showing the position of Dongpan, Penglaitan and Meishan Global Stratotype Section and Point (GSSP), China. **(b)** Late Permian paleogeographic reconstruction after Ziegler et al. (1997), indicating the location of the South China block in the peri-Gondwana region. Beneath the paleogeographic map of the Nanpanjiang Basin in South China showing the position of the investigated Dongpan and Penglaitan section during late Permian times (base map modified after Wang and Jin, 2000).

dominated slope deposits. Genetically related volcanic rocks crop out in the southwestern part of the basin towards Vietnam, suggesting the proximity of a volcanic arc related to the convergence between Indochina and South China (Faure et al., 2016). The volcanism produced by this convergence is the most likely source of the analyzed volcanic ashes (Gao et al., 2013).

In Dongpan and Penglaitan, the PTB is manifested by a sharp and conformable transition from the late Permian Dalong Formation (= Talung Formation) to the basal Triassic Ziyun Formation. Late Permian rocks in these two sections are classically assigned to the Dalong Formation of Changhsingian age. However, we note that there are substantial facies differences between these two late Permian records. The Dalong Formation in Dongpan is composed of thin-bedded siliceous mudstones, numerous ash layers and minor limestone beds (Fig. 2a). This facies association is in agreement with the vast majority of reported occurrences of this formation within the South China block. The Dalong Formation is interpreted as a basinal depositional environment with restricted circulation and an estimated water depth of 200 to 500 m (He et al., 2007; Yin et al., 2007). In Guangxi and Guizhou, the thickness of the typical Dalong Formation is highly variable and ranges from a couple of meters to ca. 60 m. Rocks assigned to the Dalong Formation in Penglaitan markedly diverge from those of the typical Dalong Formation. In Penglaitan, the Dalong Formation reaches an unusual thickness of ca. 650 m and is lithologically much more heterogeneous, with a marked regressive episode in its middle part (Shen et al., 2007). Moreover, in Penglaitan the Dalong Formation contains numerous volcanogenic sandstones distributed within the entire succession, a distinctive feature when compared to other sections. Only the lower part of the "Dalong Formation" in Penglaitan can be unambiguously assigned to this formation. The middle and upper part of this section are notably shallower, showing cross bedding and ripple marks in the uppermost 30 m of the Permian, which are underlain by upper shoreface to foreshore facies deposits containing coal seams and abundant plant fossils (Shen et al., 2007). The uppermost part of the Dalong Formation was deposited in relatively deep water settings that comprise thin-bedded dark-grey limestone intercalated with thick volcanogenic sandstones and thin volcanic ash beds (Fig. 3a). All associated volcanogenic sandstones were deposited by geologically instantaneous turbidites, mainly reflecting the basal part (Bouma A–B sequence) of such gravity flow deposits. Gradual accumulations and sediment mixing are restricted to sands bars occurring in the middle part of the section, in association with coal seams during an intervening regressive episode. Hence, the volcanogenic sandstones from the top of the Dalong Formation in Penglaitan may not suffer from substantial sediment reworking and mixing and do not represent substantial cumulative amounts of time relative to the interlayered shales and thin-bedded limestones. The depositional setting of Penglaitan is interpreted as that of a fault-bounded block successively thrown down and up. Hence, Penglaitan stands in marked contrast with the homogenous deeper water facies of the typical Dalong Formation in other sections.

The conformably overlying Early Triassic rocks have been previously assigned to the Luolou Formation in both Penglaitan and Dongpan (Feng et al., 2007; He et al., 2007; Shen et al., 2012; Zhang et al., 2006). At its type locality and elsewhere in northwestern Guangxi and southern Guizhou, the

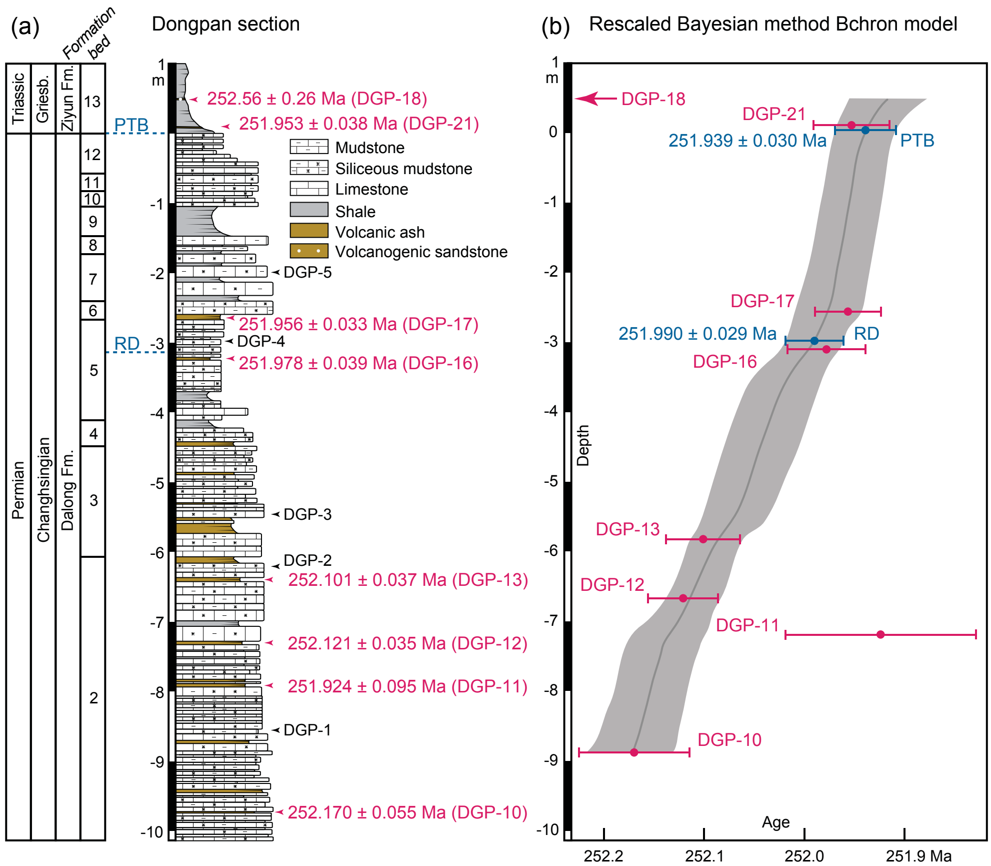

Figure 2. Stratigraphy, geochronology and Bayesian age–depth modeling for the Dongpan section from late Changhsingian to Griesbachian. **(a)** Weighted mean $^{206}Pb/^{238}U$ dates of the volcanic ash beds and volcanogenic sandstones are given in Ma. U-Pb data of DGP-21 are taken from Baresel et al. (2016). Investigated radiolarian samples (DGP-1 to DGP-5) are shown in their stratigraphic positions. **(b)** The rescaled Bayesian Bchron age–depth model is presented with its median (middle grey line) and its 95 % confidence interval (grey area). Radioisotopic dates together with their uncertainty (red horizontal bars) are presented as $^{206}Pb/^{238}U$ weighted mean dates of the dated volcanic ash beds in their stratigraphic positions. Predicted dates for the onset of the radiolarian decline (RD) and the Permian–Triassic boundary (PTB) are calculated with their associated uncertainty using the rescaled Bayesian Bchron age–depth model assuming stratigraphic superposition.

base of the Luolou Formation is invariably represented by shallow water microbial limestone. In contrast, the onset of the Triassic at Dongpan and Penglaitan is represented by ca. 30 m of laminated black shales overlain by several hundred meters of thin-bedded, mechanically laminated, medium- to light-grey limestone. In Dongpan, edgewise conglomerates and breccias are occasionally intercalated within the platy, thin-bedded limestone unit. This succession of facies illustrates a change from basinal to slope depositional environments and is identical to that of the Ziyun Formation at its type locality 3 km east of Ziyun, Guizhou Province (Guizhou Bureau of Geology and Mineral Resources, 1987). Therefore, Early Triassic rocks in Dongpan and Penglaitan are here reassigned to the Ziyun Formation, whose base is of Griesbachian age. In most sections in Guangxi and Guizhou, where latest Permian rocks are represented by the Dalong Formation, these are consistently and conformably overlain by basal black shales of the Early Triassic Ziyun Formation or the Daye Formation (e.g., Feng et al., 2015). In these downthrown blocks, the effects of the Permian–Triassic global regression were negligible in comparison to those observed in adjacent, up-thrown blocks that recorded pronounced unconformities or condensation.

2.2 The Dongpan section

Numerous litho-, bio- and chemo-stratigraphic studies (e.g., Feng et al., 2007; He et al., 2007; Luo et al., 2008; Zhang et al., 2006) have been published on the Dongpan section during the last two decades. However, the volcanic ash beds of this continuous PTB section have never been dated. The classic lithostratigraphic subdivisions of the Dongpan section (bed 2 to 13; indicated in Fig. 2a) (Meng et al., 2002) can easily be recognized in the field. Based on the conodont alteration index (CAI), Luo et al. (2011) established that the section shows only a low to moderate thermal overprint equivalent to a maximal burial temperature of 120 °C. Our own

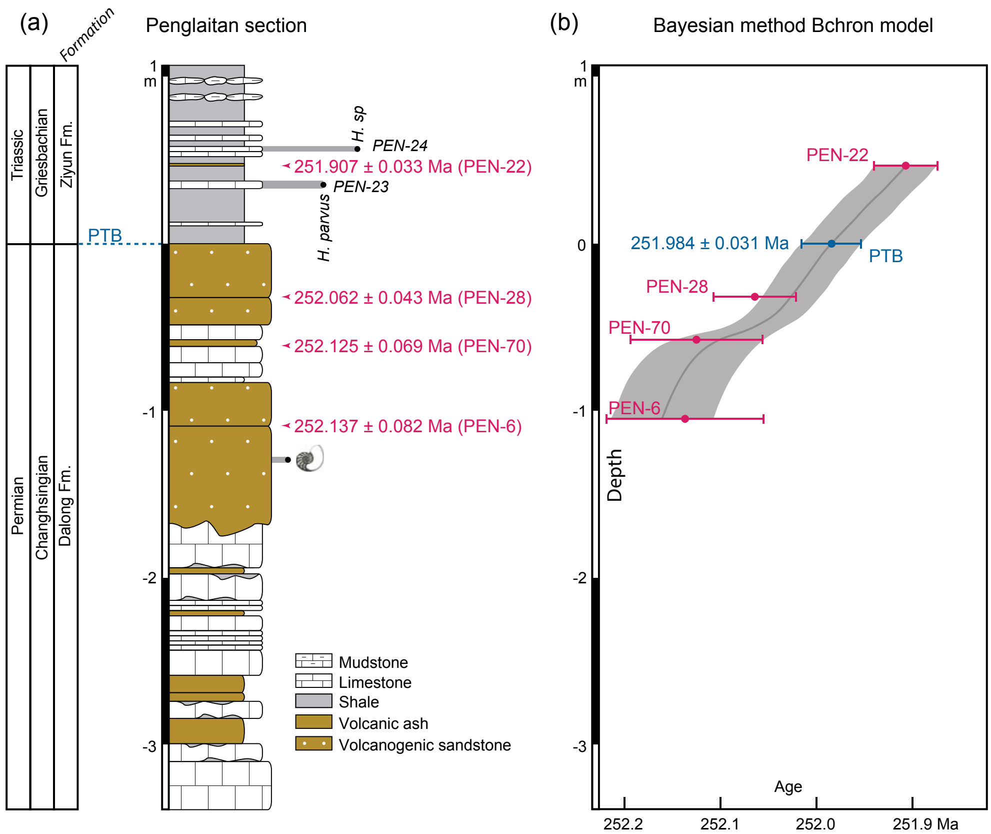

Figure 3. Stratigraphy, geochronology and Bayesian age–depth modeling for the Penglaitan section from late Changhsingian to Griesbachian. **(a)** Weighted mean $^{206}Pb / ^{238}U$ dates of the volcanic ash beds and volcanogenic sandstones are given in Ma. U-Pb data of PEN-28 and PEN-22 are taken from Baresel et al. (2016). Investigated conodont samples (PEN-23 and PEN-24; see also Sect. S5) and first occurrence of Triassic conodonts are shown in their stratigraphic positions. A poorly preserved Permian nautiloid is indicated in its stratigraphic position ca. 1.3 m below the Permian–Triassic boundary (PTB). **(b)** The rescaled Bayesian Bchron age–depth model is presented with its median (middle grey line) and its associated 95 % confidence interval (grey area). Radioisotopic dates together with their uncertainty (red horizontal bars) are presented as $^{206}Pb / ^{238}U$ weighted mean dates of the dated volcanic ash beds in their stratigraphic positions. Predicted date for the PTB is calculated with its associated uncertainty using the rescaled Bayesian Bchron age–depth model assuming stratigraphic superposition.

estimation of the CAI of conodont elements obtained from the same beds points toward values around 3, thus confirming the estimation of Luo et al. (2011).

Beds 2 to 5 consist of thin (dm to cm) siliceous mudstones, mudstones, minor lenticular limestone horizons and numerous intercalated volcanic ash beds. These beds yield radiolarians, foraminifera (Shang et al., 2003), bivalves (Yin, 1985), ammonoids (Zhao et al., 1978), brachiopods (He et al., 2005), ostracods (Yuan et al., 2007), and conodonts (Luo et al., 2008) of Changhsingian age. Chinese authors have provided very detailed studies of radiolarian occurrences from the top of the Dongpan section, documenting about 160 species belonging to 50 genera (Feng et al., 2007; Wu et al., 2010; Zhang et al., 2006). Most of these radiolarians belong to the *Neoalbaillella optima* assemblage zone of late Changhsingian age (Feng and Algeo, 2014), although it is unclear whether some of the Permian taxa reported from the top of the section by previous authors (i.e. above bed 6; Feng et al., 2007) still belong to this assemblage or to a provisional ultimate Permian biozone (Xia et al., 2004).

We collected five samples with visible radiolarians (DGP-1 to DGP-5; see Fig. 2a) for this study. Our goal was not to duplicate the detailed faunal studies performed at Dongpan by previous authors but essentially to correlate these previous results with our U-Pb ages using own radiolarian data. A selection of well-preserved taxa is illustrated in Sect. S4. We also report the occurrence of morphotypes belonging to the genus *Hegleria*, which was previously reported from the section but not illustrated. Our data confirm that radiolarians of the Dongpan section belong to the *Neoalbaillella optima* assemblage zone.

The conodont fauna obtained from beds 3 and 5 was assigned to the *Neogondolella yini* interval zone by Luo et al. (2008). *Neogondolella yini* is also a characteristic species of the UAZ1 zone, which is the oldest zone of a new high-accuracy zonation around the PTB constructed by means of unitary associations (Brosse et al., 2016). Bed 6 is composed of a yellow fine-grained volcanic ash bed and thin-bedded siliceous mudstone. Beds 7 to 12 contain more frequent mudstone and yield a diverse Permian fauna (Feng et al., 2007; He et al., 2007; Yin et al., 2007). Additionally, He et al. (2007) showed that end-Permian brachiopods underwent a size reduction in the uppermost beds of the Dalong Formation, which they linked with a regressive trend.

The sharp and conformable base (bed 13) of the Early Triassic Ziyun Formation consists of brown-weathering black shales containing a few very thin (mm to cm) volcanic ash beds and volcanogenic sandstones. Previous studies did not recognize how recent weathering superficially altered these black shales. Bed 13 contains abundant bivalves and ammonoids of Griesbachian age (Feng et al., 2007; He et al., 2007), which are also known from other sections where the equivalent black shales are not weathered. Therefore, the formational boundary placed between beds 12 and 13 is reasonably well-constrained in terms of paleontological ages. Even in the absence of any close conodont age control, this boundary has been unanimously acknowledged as the PTB in all previous contributions, thus emphasizing the significance of this formational change.

2.3 The Penglaitan section

The Penglaitan section is well known for its Guadalupian–Lopingian boundary (Capitanian–Wuchiapingian GSSP; Jin et al., 2006; Shen et al., 2007). However, the part of the section that straddles the PTB has not been the focus of any detailed published work. Shen et al. (2007) report Changhsingian *Peltichia zigzag–Paryphella* brachiopod assemblage from a volcanogenic sandstone bed at ~ 28 m below the PTB. In addition, *Palaeofusulina sinensis* is abundant in the uppermost limestone units of the Dalong Formation and conodonts in the topmost part were assigned to the *Clarkina yini* Zone. A poorly preserved Permian nautiloid was recovered from the volcanogenic sandstone 1.3 m below the PTB (Fig. 3a). About 0.3 m above the PTB, concretionary, thin-bedded micritic layers intercalated within the basal black shales of the Ziyun Formation yielded one P1 element of *Hindeodus parvus* (Fig. 3a; see also Sect. S5). Pending the age confirmation of new paleontological data, and in full agreement with Shen et al. (2007), we place the PTB at this sharp but conformable formational boundary.

3 Methods

3.1 CA-ID-TIMS analysis

Sample preparation, chemical processing and U-Pb CA-ID-TIMS zircon analyses were carried out at the University of Geneva. Single zircon grain dates were produced relative to the EARTHTIME ^{202}Pb-^{205}Pb-^{233}U-^{235}U tracer solution (Condon et al., 2015). All uncertainties associated with weighted mean ^{206}Pb / ^{238}U ages are reported at the 95 % confidence level and given as $\pm x/y/z$, with x as analytical uncertainty, y including tracer calibration uncertainty, and z including ^{238}U decay constant uncertainty. The tracer calibration uncertainty of 0.03 % (2σ) has to be added if the calculated dates are to be compared with other U-Pb laboratories not using the EARTHTIME tracer solution. The ^{238}U decay constant uncertainty of 0.11 % (2σ) should be used if compared with other chronometers such as Ar-Ar. All ^{206}Pb / ^{238}U single-grain ages have been corrected for initial ^{230}Th-^{238}U disequilibrium assuming Th/U$_{\mathrm{magma}}$ of 3.00 ± 0.50 (1σ). This should best reflect the Th/U of the whole rock and is identical to the Th/U$_{\mathrm{magma}}$ used by Burgess et al. (2014) for the Meishan ash beds in order to provide an unbiased comparison of the Dongpan, Penglaitan and Meishan chronology. Th-corrected ^{206}Pb / ^{238}U dates are on average 80 ka older than the equivalent uncorrected dates when applying this correction, but changes in the Th/U$_{\mathrm{magma}}$ have only minor effects on the deposition ages of the Dongpan and Penglaitan volcanic beds. Compared to the Th/U$_{\mathrm{magma}}$ of 3.00 ± 0.50 (1σ) used in this study, they would become max. 11 kyr younger with Th/U$_{\mathrm{magma}}$ of 2.00 ± 0.50 (1σ) and max. 7 kyr older with Th/U$_{\mathrm{magma}}$ of 4.00 ± 0.50 (1σ). All Th-corrected ^{206}Pb / ^{238}U dates are presented as mean ages of selected zircon populations and their associated $\pm 2\sigma$ analytical uncertainties in Figs. 2 and 3, and as single-grain ^{206}Pb / ^{238}U age ranked distribution plots in Fig. 4. The full data table and analytical details are given in Sect. S2.

3.2 Bayesian chronology

In this study we use Bayesian interpolation statistics to establish a probabilistic age model based on our high-precision U-Pb zircon dates of each individual ash bed and its stratigraphic position, as it is incorporated in the free Bchron R software package (Haslett and Parnell, 2008; Parnell et al., 2008) to constrain the chronological sequence and sedimentation history of the investigated sections. By assuming normal distribution of our U-Pb dates within one sample and based on the principle of stratigraphic superposition, which requires that any stratigraphic point must be younger than any point situated below in the stratigraphic sequence, it models the age and its associated 95 % confidence interval for any depth point within the studied sedimentary sequence. The model is based on the assumption of random variability of sediment accumulation rate, yielding a family of dispersed piecewise monotonic sediment accumulation models between each dated stratigraphic horizon. The number of such accumulation models is inferred by a Poisson distribution, and the size of the sediment accumulation rates by a gamma distribution. The strength of this approach is its flexibility that allows changes in sediment accumulation rate from zero (hiatus in sedimentation) to very large values (sedimentation event at high rate). In contrast to standard linear regression models, this approach leads to more realistic

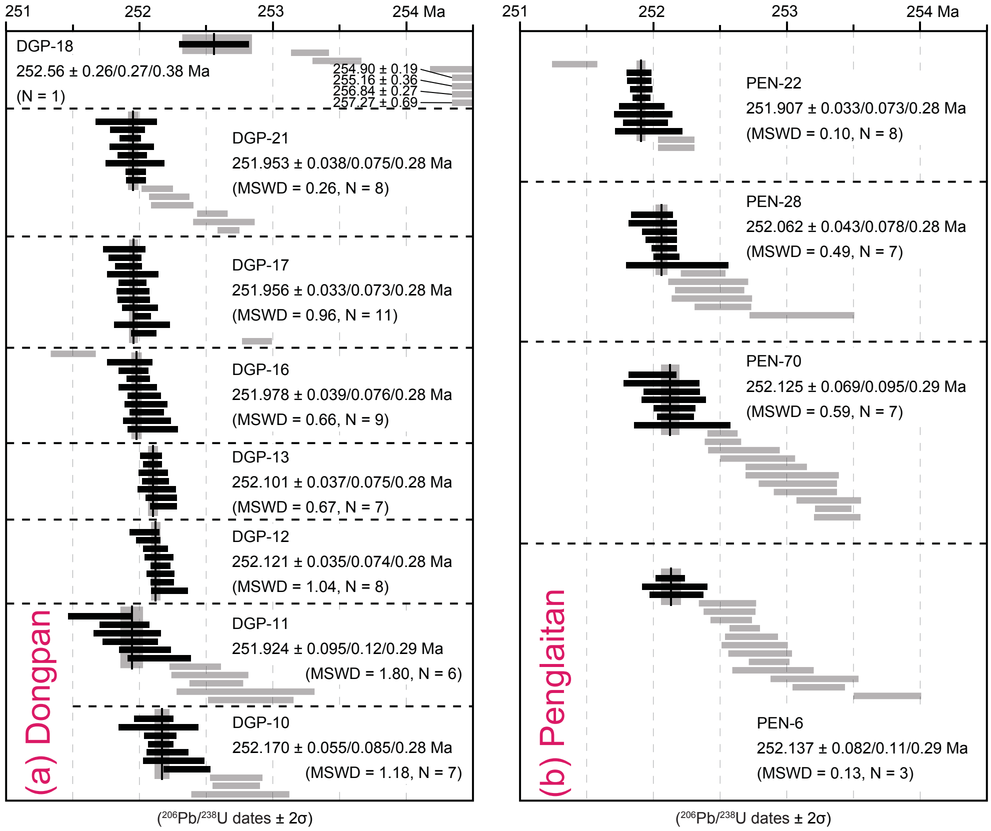

Figure 4. Single-grain zircon analysis and ^{206}Pb / ^{238}U weighted mean dates for **(a)** Dongpan and **(b)** Penglaitan volcanic ash beds and volcanogenic sandstones. U-Pb data of DGP-21, PEN-28 and PEN-22 are taken from Baresel et al. (2016). Each horizontal bar represents a single zircon grain analysis including its 2σ analytical (internal) uncertainty, whereas grey bars are not included in the weighted mean calculation. Vertical lines represent the weighted mean age, with the associated 2σ uncertainty (in grey). Uncertainty in the weighted mean dates is reported as 2σ internal, 2σ external uncertainty including tracer calibration and 2σ external uncertainty including ^{238}U decay constant uncertainty; MSWD – mean square of weighted deviates.

uncertainty estimates, with increasing uncertainty at growing stratigraphic distance from the dated layers. The model also detects and excludes outliers, which conflict with other evidence from the same sequence in order to produce a coherent and self-consistent chronology; no predefined outlier determination is required from the user. One of the drawbacks of this Bayesian approach is that a change in the sediment accumulation rate is assumed to occur at each dated stratigraphic position, though it is unlikely that the change in sedimentation occurs exactly at the depth of a dated bed. Another drawback is that the sedimentation parameters are shared across the whole sequence. In consequence, Bchron does not allow much opportunity for users to individually influence the chronology behavior.

In this study we use the Bayesian Bchron model as it is part of the Bchron package (http://cran.r-project.org/web/packages/Bchron/index.html). This model outperforms other Bayesian age–depth models, as shown by an extensive comparison conducted on radiocarbon dates from Holocene lake sediments (Parnell et al., 2011). It provides a non-parametric chronological model according to the compound Poisson–gamma model defined by Haslett and Parnell (2008), requiring the weighted mean ^{206}Pb / ^{238}U age and the stratigraphic position of the investigated ash beds as input parameters. Since the Bchron model was initially coded for radiocarbon dating with a commonly unknown duration of accumulation for a radiocarbon-dated bed, it also allows for the input thickness of such a horizon to be defined. However, the thickness of the geologically instantaneously deposited volcanic ashes was reduced to zero and the lithostratigraphy has been rescaled in order to remove the thickness of the volcanic horizons and to produce a more accurate age–depth model (Figs. 2a and 3a; see also Sect. S3). The technical details were given in Haslett and Parnell (2008). The Bchron model uses a Markov chain Monte Carlo (Brooks et al., 2011) rejection algorithm which proposes model parameters and accepts or rejects them in order to produce probability distributions of dates for a given depth that match likelihood and do not violate the principle of stratigraphic superposition. In order to create an adequate number of accepted samples, the model was run for 10 000 iterations. The Bchron R scripts of Dongpan, Penglaitan and Meishan are provided in Sect. S3.

4 Samples

In total, 12 volcanic ash beds and volcanogenic sandstones were sampled from the Dalong Formation of late Permian age and from the overlying Ziyun Formation of Early Triassic age at Dongpan and Penglaitan (see Sect. S1). Most of the dated samples exhibit ^{206}Pb / ^{238}U age dispersions that exceed the acceptable scatter from analytical uncertainty and are interpreted as reflecting magmatic residence or a combination of the latter with sedimentary recycling. Only in two cases (DGP-16, PEN-22) do we find single-grain analyses younger than our suggested mean age and interpret them as unresolved Pb loss since they violate the stratigraphic order established by the chronology of the volcanic ash beds.

At Dongpan, six fine- to medium-grained volcanic ash beds (DGP-10, DGP-11, DGP-12, DGP-13, DGP-16 and DGP-17) in the uppermost 10 m of the Dalong Formation, one fine-grained ash bed (DGP-21) just 10 cm above the base of the Ziyun Formation, and one thin-bedded volcanogenic sandstone (DGP-18) 40 cm stratigraphically higher were collected for geochronology. At Penglaitan, the basal part of a 25 cm thick volcanogenic sandstone (PEN-6), one thin-layered volcanic ash bed (PEN-70) and the base of a 30 cm thick volcanogenic sandstone (PEN-28), all together representing the uppermost 1.1 m of the Dalong Formation, were dated. A single fine-grained and extremely thin (2–3 mm) volcanic ash bed (PEN-22) was sampled 50 cm above the base of the Ziyun Formation and thus closely brackets the formational boundary. U-Pb CA-ID-TIMS geochronology following procedures described above and in the Appendix was applied to a number of single crystals of zircon extracted from these volcanic beds. Trace element and Hf isotopic compositions of these dated zircons will be presented elsewhere. Stratigraphic positions of volcanic ash beds at Dongpan and Penglaitan and weighted mean ^{206}Pb / ^{238}U dates of individual zircon grains for the samples below are given in Figs. 2 and 3.

5 Results

The U-Pb isotopic results are presented in Fig. 4 as ^{206}Pb / ^{238}U age ranked plots for each individual sample and in Table S1 (Sect. S2).

5.1 U-Pb age determinations from the Dongpan section

5.1.1 Sample DGP-10

This volcanic ash bed was sampled 9.7 m below the formational boundary. All 10 dated zircons are concordant within analytical error, where the seven youngest grains define a cluster with a weighted mean ^{206}Pb / ^{238}U age of $252.170 \pm 0.055/0.085/0.28$ Ma (mean square of weighted deviates (MSWD) = 1.18) for the deposition of DGP-10.

5.1.2 Sample DGP-11

This volcanic ash bed was sampled 7.9 m below the formational boundary. Eleven zircon crystals were analyzed, resulting in scattered ^{206}Pb / ^{238}U dates of 251.662 ± 0.263 to 252.915 ± 0.352 Ma. The six youngest zircons yield a weighted mean ^{206}Pb / ^{238}U age of $251.924 \pm 0.095/0.12/0.29$ Ma (MSWD = 1.80) that is too young with respect to the stratigraphic sequence defined by over- and underlying ash beds. Therefore, we have to assume that abundant unresolved lead loss affected these zircons, despite application of the same chemical abrasion procedure as for all other samples. It is worth noting that all zircons from DGP-11 were almost completely dissolved after chemical abrasion and show elevated ^{206}Pb / ^{238}U age uncertainties of ~ 0.30 Ma compared to other volcanic ash beds from Dongpan.

5.1.3 Sample DGP-12

This volcanic ash bed was sampled 7.3 m below the formational boundary. The weighted mean age of $252.121 \pm 0.035/0.074/0.28$ Ma (MSWD = 1.04) is derived from eight concordant grains representing the youngest zircon population of this ash bed.

5.1.4 Sample DGP-13

This volcanic ash bed was sampled 6.4 m below the formational boundary. Analyses of seven individual zircons yield a statistically significant cluster with a weighted mean ^{206}Pb / ^{238}U age of $251.101 \pm 0.037/0.075/0.28$ Ma (MSWD = 0.67) representing the youngest zircon population of this ash bed.

5.1.5 Sample DGP-16

This volcanic ash bed was sampled 3.2 m below the formational boundary. Nine zircons yield a weighted mean ^{206}Pb / ^{238}U age of $251.978 \pm 0.039/0.076/0.28$ Ma (MSWD = 0.66). The youngest grain shows unresolved lead loss and was discarded because it violates the stratigraphic superposition. Incorporating this zircon into the mean age calculation would also lead to a statistically flawed MSWD of 4.80.

5.1.6 Sample DGP-17

This volcanic ash bed was sampled 2.7 m below the formational boundary. A total of 11 zircons define a weighted mean ^{206}Pb / ^{238}U age of $251.956 \pm 0.033/0.073/0.28$ Ma (MSWD = 0.96). One single zircon displays inheritance with an ^{206}Pb / ^{238}U age of 252.896 ± 0.108 Ma and was consequently excluded from the weighted mean age calculation.

5.1.7 Sample DGP-21

This volcanic ash bed was sampled 0.1 m above the formational boundary. Fourteen zircons were dated, among which the eight youngest yield a cluster with a weighted mean ^{206}Pb / ^{238}U age of 251.953 ± 0.038/0.075/0.28 Ma (MSWD = 0.26). The six oldest grains display an inherited component as suggested by their scattered ^{206}Pb / ^{238}U dates ranging from 252.145 ± 0.120 to 252.715 ± 0.084 Ma. The U-Pb data of DGP-21 have already been published in a companion study (Baresel et al., 2016) that deals with the stratigraphic correlation of ash beds straddling the PTB in deep- and shallow-marine successions of the Nanpanjiang Basin.

5.1.8 Sample DGP-18

This bed was sampled 0.5 m above the formational boundary. The re-sedimented nature of this volcaniclastic bed is reflected in the ^{206}Pb / ^{238}U zircon ages ranging from 252.559 ± 0.261 to 257.274 ± 0.689 Ma. This sample was excluded from the age–depth model because it clearly violates the stratigraphic superposition.

5.2 U-Pb age determinations from the Penglaitan section

5.2.1 Sample PEN-6

PEN-6 comes from the base of a volcanogenic sandstone. It was sampled 1.1 m below the formational boundary. Fifteen zircon grains were dated. The three youngest grains define a weighted mean ^{206}Pb / ^{238}U age of 251.137 ± 0.082/0.11/0.29 Ma (MSWD = 0.13). Because zircon dates from this bed spread over almost 2 Myr, recycling of older volcanic material via sedimentary processes appears more likely than via magmatic recycling.

5.2.2 Sample PEN-70

This volcanic ash bed was sampled 0.6 m below the formational boundary. Eighteen zircon grains were analyzed. As in the case of PEN-6, they yield a scatter of ^{206}Pb / ^{238}U dates spanning 1.5 Myr, ranging from 251.994 ± 0.169 to 253.371 ± 0.165 Ma. The weighted mean age of 252.125 ± 0.069/0.095/0.29 Ma (MSWD = 0.59) for the deposition of this ash bed is calculated by using the seven youngest concordant grains.

5.2.3 Sample PEN-28

This sample was taken 0.3 m below the formational boundary. It is derived from the base of a 30 cm thick volcanogenic sandstone which represents the youngest Permian bed in Penglaitan. Analyses of seven zircon grains yield a cluster with a weighted mean ^{206}Pb / ^{238}U age of 252.062 ± 0.043/0.078/0.28 Ma (MSWD = 0.49), reflecting the last crystallization phase of this zircon population. Six older grains, ranging from 252.364 ± 0.156 to 253.090 ± 0.375 Ma, indicate either magmatic or sedimentary recycling. The U-Pb data of PEN-28 have already been published in Baresel et al. (2016).

5.2.4 Sample PEN-22

This 2 mm thick volcanic ash bed was sampled 0.5 m above the formational boundary. Eight zircons yield a weighted mean ^{206}Pb / ^{238}U age of 251.907 ± 0.033/0.073/0.28 Ma (MSWD = 0.10). One zircon grain shows a significantly younger age suggesting lead loss. Two slightly older grains reflect noticeable pre-eruptive crystallization. Incorporation of these grains into the weighted mean calculation would lead to an excessive MSWD of 3.6 and 1.9, respectively.

However, we noticed that some volcanic ash beds and volcanogenic sandstones in these sections show a large age dispersion of up to 2 Myr, incompatible with recycling of zircon that previously crystallized within the same magmatic system and became recycled into later melt batches, leading to dispersion of dates of a few 100 kyr (e.g., Broderick et al., 2015; Samperton et al., 2015), but pointing to sedimentary reworking. The U-Pb data of PEN-22 have already been published in Baresel et al. (2016).

5.3 Age–depth models

Figure 5 shows a comparison of three different age–depth models based on linear interpolation, cubic spline interpolation and Bayesian statistics, each applied to exactly the same U-Pb dataset of Dongpan (Fig. 5a) and Penglaitan (Fig. 5b). As discussed in the Methods section, the Bayesian Bchron model leads to more realistic uncertainty estimates, producing an increased uncertainty of the model age with increasing distance from the stratigraphic position of a U-Pb dated sample. Due to the well constrained U-Pb dates of Dongpan and Penglaitan, all three age–depth models predict (within uncertainty) similar ages for the PTB in Dongpan (Fig. 5a) and Penglaitan (Fig. 5b). Given that the Bayesian Bchron model evaluates the age probability distribution of each U-Pb date with respect to the other dates of the sequence, it provides a more robust and better constrained chronology, which even results in smaller uncertainties of the predicted model dates compared to the standard linear regression models (as indicated by the smaller uncertainty of the Bchron model age for the PTB in Dongpan and Penglaitan). In contrast to the other models, the Bayesian Bchron model can identify U-Pb dates that violate the principle of stratigraphic superposition, as shown for the Dongpan ash beds DGP-11 (outlier probability of 67 %) and DGP-18 (outlier probability of 100 %). Including them into the age–depth chronology of Dongpan results in unrealistic negative sediment accumulation rates,

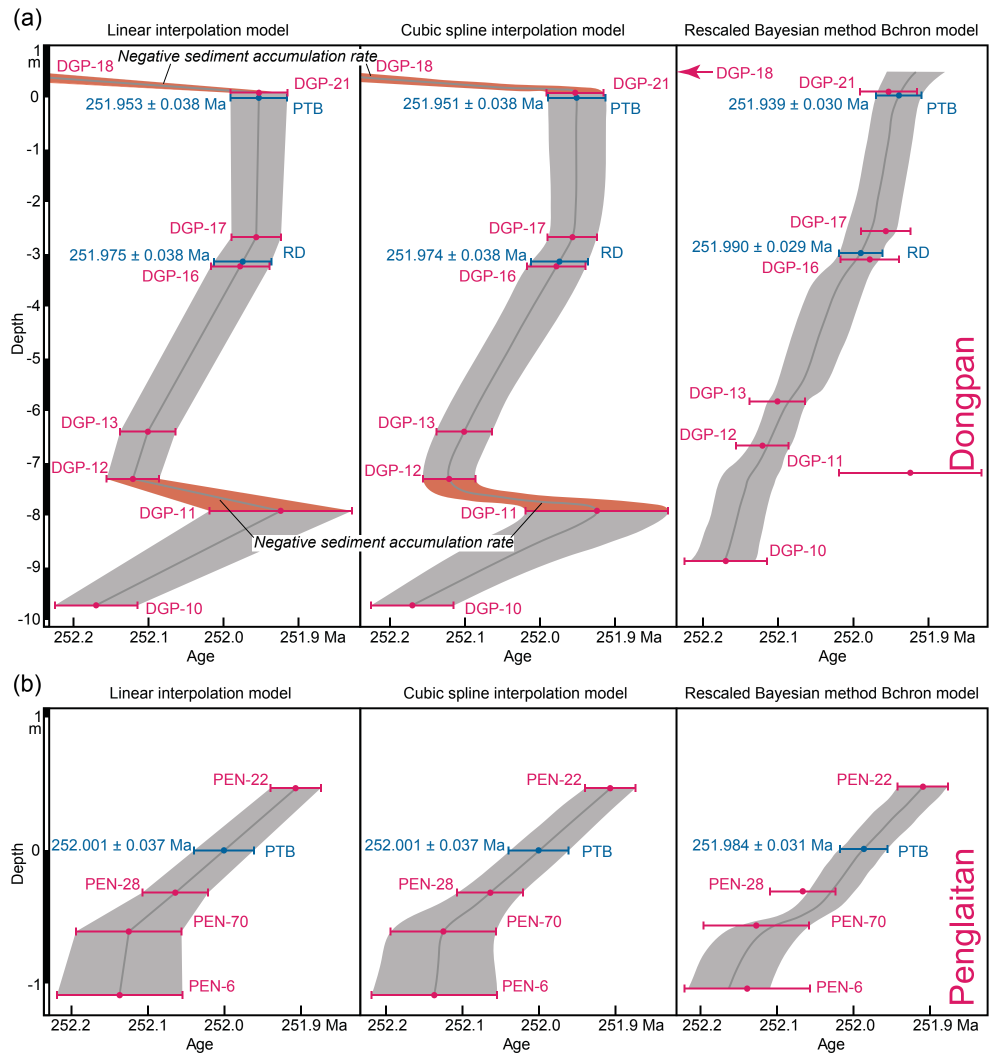

Figure 5. Comparison of the different age–depth models based on linear interpolation, cubic spline fit and Bayesian statistics for **(a)** Dongpan and **(b)** Penglaitan. Each age–depth model is presented with its median (middle grey line) and its associated 95 % confidence interval (grey area). Radioisotopic dates, used in the age–depth models, together with their uncertainty (red horizontal bars) are presented as ^{206}Pb / ^{238}U weighted mean dates of the Dongpan and Penglaitan volcanic ash beds and volcanogenic sandstones in their stratigraphic positions. U-Pb data of DGP-21, PEN-28 and PEN-22 are taken from Baresel et al. (2016). Predicted dates (blue horizontal bars) for the onset of the radiolarian decline (RD) and the Permian–Triassic boundary (PTB) in Dongpan and Penglaitan are calculated with their associated uncertainty using the different age–depth models.

as reflected by the linear and cubic interpolation models for the interval between DGP-11 and DGP-12, and for the interval between DGP-21 and DGP-18 (Fig. 5a).

In all Bchron models, the thickness of the geologically instantaneously deposited volcanic ash beds was virtually removed and the lithostratigraphy has been rescaled in order to create accurate deposition rate models for the investigated sedimentary successions. This approach has only minor effects in the Bchron age–depth model of Dongpan, where the changes in the calculated age of the PTB and the radiolarian decline (RD) are negligible (see Sect. S3), mainly due to the limited thickness (max. 8 cm) of the volcanic horizons in Dongpan. The Bchron model of Penglaitan would be much more affected by such a rescaling if the thickness of the volcanogenic sandstones were also removed, but it is not clear whether each volcanogenic sandstone represents only one "instantaneous" turbidity current event or might reflect a series of several turbidite deposits over a certain time. Hence, also in Penglaitan only the thickness of the volcanic ash beds was removed. However, the relative substantial thickness of "instantaneously" deposited turbiditic volcanogenic sandstone at the top of the Penglaitan section may indeed induce some distortions in the Bchron model. Facies analysis did not reveal any signs of an omission surface at the formational boundary, but the strong contrast in sediment accumulation rates between the "instantaneous" deposition of the last Permian bed and the much slower accumulation of next overlying black shales likely generates a distortion of the Bchron model at the formational boundary. Hence, the Bchron model derived from Dongpan is certainly more reliable than that derived from Penglaitan.

The aim for applying Bayesian age modeling to the dated volcanogenic beds from these two sections was to obtain an age model for the PTB. The age–depth models yield ages of 251.939 ± 0.030 Ma (Dongpan; Figs. 2a and 5a) and of 251.984 ± 0.031 Ma (Penglaitan; Figs. 3b and 5b) for the lithological boundary between the Dalong and Ziyun Formation in both sections. These two ages overlap within uncertainties and thus demonstrate the synchronicity of the PTB in the two sections. Making the reasonable assumption of absence of significant gaps in these two sections, the new U-Pb dates can be used to infer sediment accumulation rates. The age–depth model of Dongpan suggests increased sediment accumulation rates in the uppermost part of the Dalong Formation from bed 6 (DGP-17) upwards. Below bed 6, calculated sediment accumulation rates appear to be relatively constant with 3.6 ± 1.2 cm kyr^{-1}, but above bed 6 they jump to 6.0 ± 2.4 cm kyr^{-1}. In Penglaitan, the sediment accumulation rate of the uppermost Dalong Formation and basalmost Ziyun Formation is significantly lower than in Dongpan with 0.7 ± 0.3 cm kyr^{-1}. Previously published U-Pb zircon geochronology from Penglaitan (Shen et al., 2011), including a weighted mean date of 252.16 ± 0.09 Ma from a volcanogenic sandstone at 26.7 m below the PTB, was not considered in our age model, since substantial improvements in the analytical protocol hamper comparing these dates with our U-Pb results.

6 Comparison of the Dongpan and Penglaitan sections with Meishan GSSP results

6.1 The change of the PTB age through analytical improvement of U-Pb dating

The first geochronological studies in the GSSP at Meishan D have been carried out on a volcanic ash in bed 25, whose base starts 4 cm below the formational PTB, by U-Pb sensitive high-resolution ion microprobe (SHRIMP) analysis of zircons yielding a ^{206}Pb / ^{238}U age of 251.2 ± 3.4 Ma (Claoué-Long et al., 1991) and by ^{40}Ar/^{39}Ar dating of sanidine at 249.91 ± 0.15 Ma (Renne et al., 1995). However, these dates are either not sufficiently precise to allow calibrating magmatic and biological timescales at resolution adequate for both groups of processes or are biased by a systematic age offset between the U-Pb and Ar-Ar systems of ~ 1.0 % (Schoene et al., 2006). In order to properly compare the two systems, all older ^{40}Ar/^{39}Ar data have to be corrected for the revised age of the standard Fish Canyon sanidine of 28.201 ± 0.046 Ma (Kuiper et al., 2008) and the decay constant uncertainty has to be added to U-Pb and Ar-Ar ages, which would drastically expand the ^{40}Ar/^{39}Ar age error and recalculate the ^{40}Ar/^{39}Ar age of Renne et al. (1995) to 251.6 ± 0.6 Ma. In a first detailed ID-TIMS study, U-Pb ages of mechanically abraded zircons were published by Bowring et al. (1998) for six volcanic ash beds at Meishan, placing the PTB at 251.4 ± 0.3 Ma. Though much more precise than former studies, these ages are mainly based on multi-grain zircon analyses. It was shown by Mundil et al. (2001), by confining data selection to single-crystal analyses of the same horizons, that the multi-grain approach might disguise complexity of zircon population ages which are caused by pervasive lead loss and inheritance. In a second attempt, driven by further improvements in the U-Pb ID-TIMS technique (e.g., chemical abrasion of zircon grains by hydrofluoric acid exposure to remove zircon domains with lead loss; reduced procedural common Pb blanks), the PTB extinction horizon in Meishan and Shangsi (China) was dated at 252.6 ± 0.2 Ma by Mundil et al. (2004). Unlike previous studies, Shen et al. (2011) dated larger number of zircon grains per ash bed in order to overcome inheritance, magmatic residence, and lead loss phenomena of zircon population ages. They determined the duration of the PTB extinction interval (bed 25 to bed 28 in Meishan) at 200 ± 100 kyr starting at 252.28 ± 0.08 Ma in bed 25 together with a sharp negative δ^{13}C excursion. By using the same mineral separates from identical ash beds as in Shen et al. (2011), the extinction period at Meishan was determined by Burgess et al. (2014) between 251.941 ± 0.037 Ma (bed 25) and 251.880 ± 0.031 Ma (bed 28). The differences in age and precision compared to Shen et al. (2011) reflect significant progress of the EARTHTIME community in data acquisition and reduction such as refined tracer calibration, new error propagation algorithms, and the development of the EARTHTIME ^{202}Pb-^{205}Pb-^{233}U-^{235}U tracer solution.

Figure 6 illustrates the three Bayesian age–depth models based on our U-Pb dates from Dongpan and Penglaitan compared to the latest generation of U-Pb ages from Meishan GSSP (Burgess et al., 2014). Such a comparison is possible because all the dates from these three sections were obtained with the same analytical procedures, including identical data reduction procedures, error propagation and Th correction, thus leading to closely comparable precision and accuracy of the ages. This tight temporal framework allows us to perform a quantitative comparison of the Dongpan, Penglaitan and Meishan sections in terms of lithostratigraphy, biostratigraphy and chemostratigraphy via the Bayesian statistics.

6.2 Comparison of lithostratigraphy

All three interpolated ages of the formational boundary in Dongpan (251.939 ± 0.030 Ma), Penglaitan (251.984 ± 0.031 Ma) and Meishan (251.956 ± 0.035 Ma) are in agreement within errors (Fig. 6). They support the

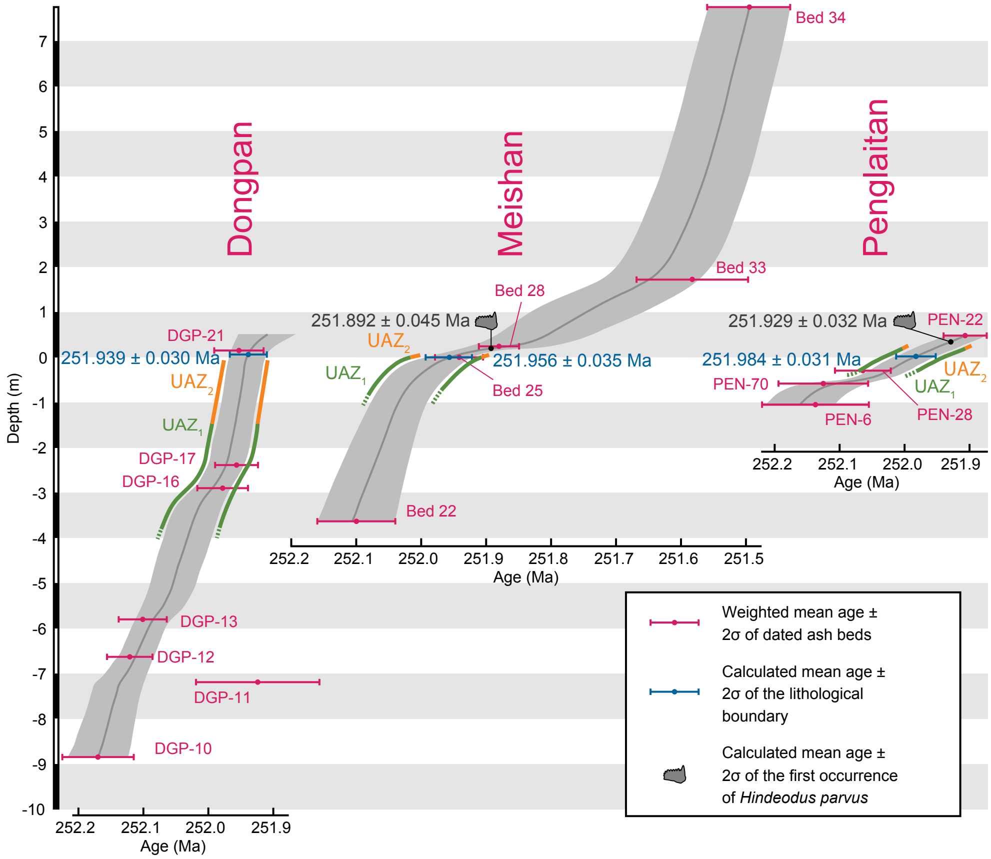

Figure 6. Comparison of Bayesian Bchron age models for Dongpan, Penglaitan and the Meishan GSSP. Predicted dates together with their uncertainty for the lithological boundaries and the first occurrence of the conodont *Hindeodus parvus* at Dongpan and Penglaitan are calculated using U-Pb ages of this study and of Baresel et al. (2016), and the U-Pb ages of Burgess et al. (2014) for Meishan. The durations of the conodont unitary association zones (UAZs) UAZ1 and UAZ2 (Brosse et al., 2016) are inferred from the Bchron age model of Meishan and projected to the model of Dongpan and Penglaitan, respectively.

synchronicity of the conformable boundary between the Dalong Formation and the Ziyun Formation in Dongpan and Penglaitan, and also demonstrate their temporal coincidence with the conformable boundary in Meishan between the Changhsing Formation and Yinkeng Formation. The age model also confirms the extreme condensation around the PTB in Meishan, with a maximal sediment accumulation rate of 0.4 cm kyr^{-1} as reported by Burgess et al. (2014) for the 26 cm thick interval between the base of bed 25 and the base of bed 28. In this respect, Dongpan and Penglaitan offer a greater potential for higher-resolution studies of environmental proxies around the PTB with maximal sediment accumulation rates for the same interval of 8.4 and 1.0 cm kyr^{-1}, respectively. The increased sediment accumulation rate above bed 6 in Dongpan is in agreement with the previously inferred sedimentary fluxes deduced from elemental chemical analyses (Shen et al., 2012). From bed 7 upward, He et al. (2007) showed a clear increase in Al_2O_3 and TiO_2, indicating increased fluxes of terrestrial input into this trough. The accompanying size reduction of brachiopods (He et al., 2007) led them to infer a regressive trend in the upper part of the Dongpan section. The ecological consequences of any regressive trend or increased clastic input might conceivably impact the diversity of marine species, but distinguishing between increased fluxes and regression remains difficult because both causes may have converging consequences.

6.3 Comparison of biostratigraphy

The PTB is defined by the FO of *H. parvus* in the Meishan GSSP in bed 27c. This definition is complicated by the suggested existence of a hardground within bed 27, which is at the position of the previously defined PTB (Chen et al., 2009). Others have suggested that the FO of *H. parvus* at Meishan is not the timing of the true evolutionary origination of this species (Jiang et al., 2011; Yuan et al., 2015). In Meishan, the FO of *H. parvus* in bed 27c is interpolated at 251.892 ± 0.045 Ma (Fig. 6) and is located 21 cm above the formational boundary which occurs between beds 24 and 25. Temporally coincident, the FO of *H. parvus* in Penglaitan is interpolated at 251.929 ± 0.032 Ma (Fig. 6) and is located 33 cm above the formational boundary. With respect to formational boundaries, the higher stratigraphic position of the FO of *H. parvus* in Penglaitan than in Meishan is to be expected because of the higher sediment accumulation rate. However, in Meishan *H. parvus* first occurs 64 ± 56 kyr and in Penglaitan 53 ± 46 kyr after the formational boundary, indicating perfect synchronicity within our temporal resolution. In Dongpan, the lack of conodont bearing beds around the PTB hampers testing the synchronicity of the FO of *H. parvus* between Dongpan and the two other sections.

Brosse et al. (2016) established a new and robust conodont zonation based on unitary associations around the PTB in South China that includes the Meishan GSSP. This zonation contains six unitary association zones (UAZs), with the PTB falling into the separation interval between UAZ2 (bed 25) and UAZ3 (bed 27a–d). This new zonation also places the UAZ-based PTB in Meishan closer to the conformable boundary between the Changhsing Formation and the Yinkeng Formation than the FO of *H. parvus* (bed 27c) does. Available conodont data from Meishan allow the assignment of bed 24a–e to UAZ1 (UAZ1 might reach further down as indicated by a dashed line in Fig. 6), bed 25 to UAZ2, bed 27a–d to UAZ3 and bed 28 to UAZ4 (Brosse et al., 2016). The stratigraphic thickness comprised between the base of UAZ1 and the top of UAZ4 amounts to 1.22 m. By using the three-section age–depth models, we attempted to project the respective thickness corresponding to the UAZ1–UAZ4 interval in Meishan onto the two other sections. This projection resulted into a pronounced, artificial lengthening of UAZs in Dongpan and Penglaitan. UAZ1 is the penultimate Permian conodont UAZ in Meishan (Brosse et al., 2016). When projected onto the age–depth models of Dongpan and Penglaitan, this UAZ1 is artificially expanded and even crosses the PTB in Penglaitan (Fig. 6). In Penglaitan, the last Permian UAZ2 projects correctly above UAZ1 without overlap but is completely within the Triassic. The cause of these contradictions stems from the irreconcilable conjunction of (i) extreme condensation in Meishan, (ii) high evolutionary rates of conodonts, and (iii) the ~ 40 ka precision of the last generation of U-Pb dates.

In Dongpan, the onset of a protracted radiolarian diversity decline in bed 5 reported by Feng and Algeo (2014) is here interpolated at 251.990 ± 0.029 Ma, occurring 51 ± 42 kyr before the formational boundary (Fig. 2). Excess SiO_2 values of this bed (Shen et al., 2012) suggest a genuine diversity pattern at the local scale, which seems to be unrelated to any substantial change or trend in the local redox conditions (as shown by Co / Al, Cr / Al, Cu / Al and V / Al measurements of He et al., 2007).

6.4 Comparison of chemostratigraphy

Organic carbon isotope chemostratigraphy of Dongpan (Fig. 7) extending from the Permian bed 5 to the Triassic bed 13 was provided by Zhang et al. (2006) and for Meishan (Fig. 7) extending from the Permian bed 24 to the Triassic bed 29 by Cao et al. (2002). The correlation of these $\delta^{13}C_{org}$ records by Zhang et al. (2006), based on the occurrence of ash beds in both sections, is largely over-interpreted. With the exception of a short negative excursion followed by a more prominent positive excursion between beds 9 and 11, the Permian part of the $\delta^{13}C_{org}$ record in Dongpan is relatively stable and oscillates between -28 and -27 ‰. With the exception of a negative excursion culminating in beds 25 and 26, the Permian part of the $\delta^{13}C_{org}$ record in Meishan shows a sustained positive trend from -30 to -26 ‰. The basal Triassic part of these two records is also incompatible in that they display opposite trends. With the possible exception of the Xinmin section (J. Shen et al., 2013), the $\delta^{13}C_{org}$ record of Dongpan does not correlate with that of any other South Chinese section, but even Xinmin shows a ~ 3 ‰ offset of the base trend in comparison to Dongpan. However, we note that in Meishan an abrupt decline in $\delta^{13}C_{carb}$ occurs in bed 24e at 251.950 ± 0.042 Ma (Burgess et al., 2014) and slightly above in bed 26 in $\delta^{13}C_{org}$ at 251.939 ± 0.032 Ma, which is temporally coincident with the main negative $\delta^{13}C_{org}$ excursion in bed 9 in Dongpan at 251.956 ± 0.030 Ma. The second smaller negative $\delta^{13}C_{org}$ excursion at the PTB in Dongpan at 251.941 ± 0.030 Ma and in Meishan at 251.892 ± 0.045 Ma cannot be distinguished within uncertainty from the main excursion, which hampers the correlation of the $\delta^{13}C_{org}$ records based on U-Pb ages. However, interpreting organic carbon records requires the simultaneous analysis of palynofacies, which are not documented in Dongpan. Shen et al. (2012) also showed that the total organic carbon (TOC) never exceeds 0.2 %, thus indicating a generally poor preservation of the organic matter in this section. As shown by Shen et al. (2012), this preservation bias is further supported by coincident peaks in both terrestrial (spore and pollens) and marine (algae and acritarchs) organic material (see Fig. 7). This uneven preservation of the organic matter further hampers the understanding of the $\delta^{13}C_{org}$ signal in Dongpan. More generally, the consistency and lateral reproducibility of the late Permian carbonate and organic carbon isotope records in South China remain equivocal (e.g., S. Z. Shen et al., 2013). These records are probably influenced by the local graben and horst paleotopography that hampered efficient circulation of water masses with the open ocean, thus reflecting more local than global changes.

6.5 Comparison of astrochronology

Sedimentary cycles driven by orbital forcing (100 kyr eccentricity cycles) were inferred by Peng et al. (2008) on the basis of Ce/La fluctuations in Dongpan. These cycles were also used by Feng and Algeo (2014) to calibrate their radiolarian extinction and survival intervals. The duration of these two intervals amounts to ~ 260 kyr (see their Fig. 5). For the same stratigraphic interval, our U-Pb ages (interval

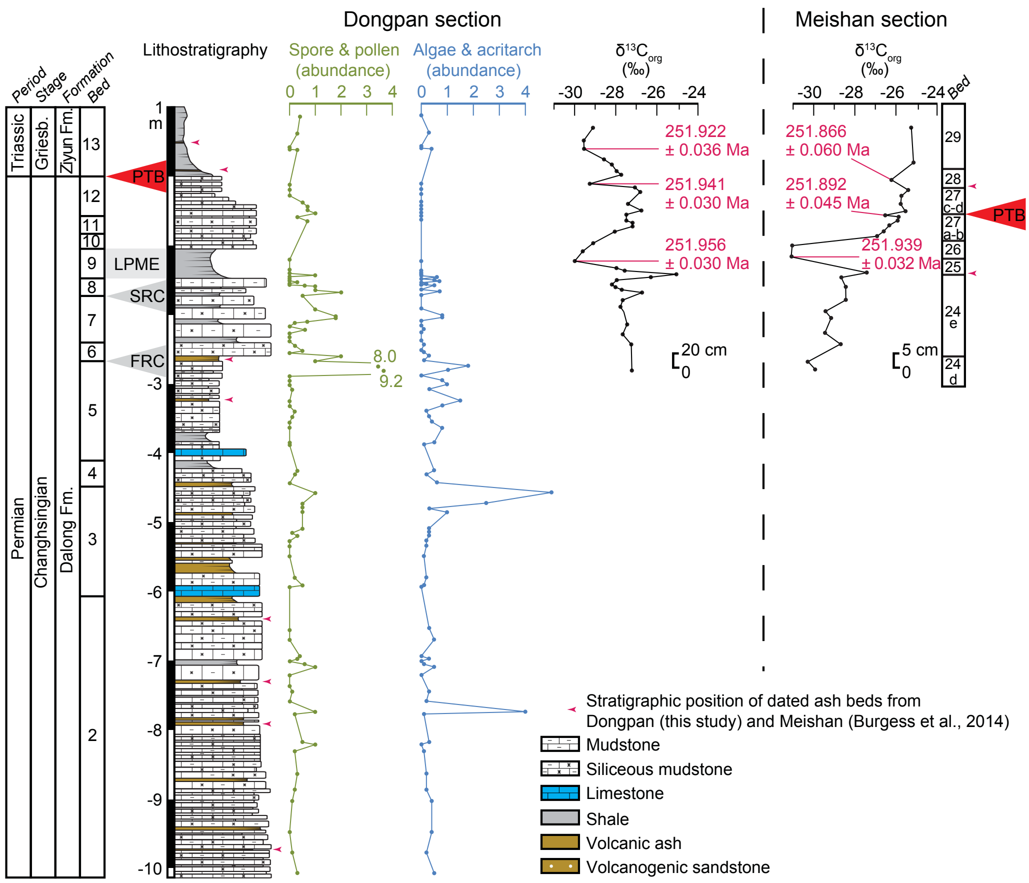

Figure 7. Comparison of the organic carbon isotope chemostratigraphy of Dongpan (Zhang et al., 2006) with that of Meishan (Cao et al., 2002). Dates and their associated uncertainty for the negative carbon isotope excursions in both sections are revealed from the Bayesian Bchron age models of Dongpan and Meishan, respectively. Abundance of spores and pollen, as well as algae and acritarchs (i.e., spores per 100 cm^2 of soil) in Dongpan, is from Shen et al. (2012). Stratigraphic positions of the first radiolarian crisis (FRC) and second radiolarian crisis (SRC) (after Feng et al., 2007), the latest Permian extinction event (LPME) in Dongpan and the Permian–Triassic boundary (PTB) in both sections are indicated as well. Meishan section thickness is not to scale with the Dongpan section.

from DGP-16 to DGP-21) indicate a much shorter duration of max. 75 kyr. It is not clear whether this chemical cyclicity might represent either precession instead of eccentricity cycles or rather a local signal of the sedimentary-chemical system. Huang et al. (2011) produced an astrochronological timescale across the PTB in China and Austria with an estimated duration of 700 kyr for the extinction interval. However, the extinction interval in their study is too long and ranges from the start of the *Neogondolella meishanensis* conodont zone to the base of the *Isarcicella isarcica* zone, defining a prolonged extinction interval stretching from the top of bed 24e to the base of bed 29 in Meishan. Wu et al. (2013) reported Milankovitch cycles from late Permian strata at Meishan and Shangsi, South China, indicating a 7.793 Myr duration for the Lopingian epoch based on 405 kyr orbital eccentricity cycles. Their inferred duration of 83 kyr for the extinction interval in Meishan between the base of bed 25 and the top of bed 28 is in good agreement with the radioisotopically dated duration of 61 ± 48 kyr for the same interval (Burgess et al., 2014). This is consistent with the study of Li et al. (2016), whose astronomical-cycle tuning of spectral gamma-ray logs constrains the extinction interval in Meishan to less than 40 % of a 100 kyr eccentricity cycle (i.e., < 40 kyr).

7 Conclusions

– The comparison of our high-precision U-Pb zircon data from Dongpan and Penglaitan sections in South China with the data of Burgess et al. (2014) from Meishan D GSSP provides convincing evidence that dates elaborated through the use of the EARTHTIME ^{202}Pb-^{205}Pb-^{233}U-^{235}U tracer solution are comparable at the 0.05 % level or better even if coming from different laboratories. This fact underlines a substantially increased accuracy and precision of U-Pb ID-TIMS dating, now capable of elucidating environmental change and biotic response on a decamillennial scale.

- Applying Bayesian age modeling to sections with such high-precision time information allows for quantitative comparison of disparate information from different sections. Along with the work of Ovtcharova et al. (2015) at the Early–Middle Triassic boundary, these are the two first proof-of-concept studies adopting age–depth modeling to compare coeval sections with different fossil contents, different facies and disparate sediment accumulation rates at highest temporal resolution. We anticipate that this approach will need to become the future standard in the assessment of the geologic timescale.

- Bchron age–depth models demonstrate synchronicity of the conformable lithological boundaries in Dongpan, Penglaitan, and Meishan. These results highlight the temporal reliability of the environmental changes as expressed by formational boundaries in platform-slope and deeper water basinal sections.

- The higher sediment accumulation rates of Dongpan and Penglaitan provide a much better prospect for the high-resolution study of environmental proxies around the PTB than the condensed GSSP section in Meishan. Our age–depth models also reveal that the combination of condensed deposition with high evolutionary rates of conodonts and the ~ 30 ka resolution of the last generation of U-Pb ages makes it impossible to project stratigraphic data points or intervals of Meishan onto expanded PTB sections without distortions. This intrinsic problem of the Meishan GSSP section should stimulate the search of alternative sections with more expanded records.

- The seemingly erratic late Permian carbon isotope record in South China does not allow laterally reproducible intercalibration with the newly obtained U-Pb dates. This stands in sharp contrast with the Early Triassic carbon isotope record, which is of global significance (e.g., Galfetti et al., 2007), thus making the Early Triassic interval the ideal target of future studies that integrate chemostratigraphy, geochronology and astrochronology in a Bayesian age–depth modeling approach.

The Supplement related to this article is available online at doi:10.5194/se-8-361-2017-supplement.

Competing interests. The authors declare that they have no conflict of interest.

Acknowledgements. The authors acknowledge financial support by the Swiss NSF through projects 200020_137630 (to Urs Schaltegger) and 200021_135446 (to Hugo Bucher). Aymon Baud (Lausanne) is thanked for support in the field. Tom Algeo (Cincinnati) and Shen Shuzhong (Nanjing) are thanked for insightful discussions and for providing Excel tables of carbon isotopic data from published sections. Special thanks go to technical and scientific members of the Geneva and Zurich research groups who helped during all stages of this study. M. Schmitz and S. Burgess are gratefully acknowledged for comments and suggestions that substantially improved the manuscript.

Edited by: M. Heap
Reviewed by: M. Schmitz and S. Burgess

References

Algeo, T. J. and Twitchett, R. J.: Anomalous Early Triassic sediment fluxes due to elevated weathering rates and their biological consequences, Geology, 38, 1023–1026, doi:10.1130/G31203.1, 2010.

Alroy, J., Aberhan, M., Bottjer, D. J., Foote, M., Fürsich, F. T., Harries, P. J., Hendy, A. J. W., Holland, S. M., Ivany, L. C., Kiessling, W., Kosnik, M. A., Marshall, C. R., McGowan, A. J., Miller, A. I., Olszewski, T. D., Patzkowsky, M. E., Peters, S. E., Villier, L., Wagner, P. J., Bonuso, N., Borkow, P. S., Brenneis, B., Clapham, M. E., Fall, L. M., Ferguson, C. A., Hanson, V. L., Krug, A. Z., Layou, K. M., Leckey, E. H., Nürnberg, S., Powers, C. M., Sessa, J. A., Simpson, C., Tomasovych, A., and Visaggi, C. C.: Phanerozoic trends in the global diversity of marine invertebrates, Science, 321, 97–100, doi:10.1126/science.1156963, 2008.

Baresel, B., D'Abzac, F. X., Bucher, H., and Schaltegger, U.: High-precision time-space correlation through coupled apatite and zircon tephrochronology: an example from the Permian-Triassic boundary in South China, Geology, 45, 83–86, doi:10.1130/g38181.1, 2016.

Benton, M. J.: The origins of modern biodiversity on land, Philos. T. Roy. Soc. Lond. B, 365, 3667–3679, doi:10.1098/rstb.2010.0269, 2010.

Bowring, J. F., McLean, N. M., and Bowring, S. A.: Engineering cyber infrastructure for U-Pb geochronology: tripoli and U-Pb_Redux, Geochem. Geophys. Geosyst., 12, Q0AA19, doi:10.1029/2010gc003479, 2011.

Bowring, S. A., Erwin, D. H., Jing, G. Y., Martin, M. W., Davidek, K., and Wang, W.: U/Pb zircon geochronology and tempo of the end-Permian mass extinction, Science, 280, 1039–1045, doi:10.1126/science.280.5366.1039, 1998.

Broderick, C., Wotzlaw, J.-F., Frick, D., Gerdes, A., Günther, D., and Schaltegger, U.: Linking the thermal evolution and emplacement history of an upper-crustal pluton to its lower-crustal roots using zircon geochronology and geochemistry (southern Adamello batholith, N. Italy), Contrib. Mineral. Petr., 170, 28, doi:10.1007/s00410-015-1184-x, 2015.

Brooks, S., Gelman, A., Jones, G., and Meng, X.-L. (Eds.): Handbook of Markov Chain Monte Carlo, CRC Press, Boca Raton, Florida, USA, 619 pp., 2011.

Brosse, M., Bucher, H., and Goudemand, N.: Quantitative biochronology of the Permian-Triassic boundary in South China based on conodont Unitary Associations, Earth-Sci. Rev., 155, 153–171, doi:10.1016/j.earscirev.2016.02.003, 2016.

Burgess, S. D. and Bowring, S. A.: High-precision geochronology confirms voluminous magmatism before, during, and after Earth's most severe extinction, Sci. Adv., 1, 1–14, doi:10.1126/sciadv.1500470, 2015.

Burgess, S. D., Bowring, S. A., and Shen, S. Z.: High-precision timeline for Earth's most severe extinction, P. Natl. Acad. Sci. USA, 111, 3316–3321, doi:10.1073/pnas.1317692111, 2014.

Cao, C. Q., Wang, W., and Jin, Y.: Carbon isotope variation across Permian-Triassic boundary at Meishan section in Zhejiang province, China, Bulletin of Sciences (Chinese edition), 47, 302–306, doi:10.1360/02tb9252, 2002.

Chen, J., Beatty, T. W., Henderson, C. M., and Rowe, H.: Conodont biostratigraphy across the Permian-Triassic boundary at the Dawen section, Great Bank of Guizhou, Guizhou Province, South China: implications for the Late Permian extinction and correlation with Meishan, J. Asian Earth Sci., 36, 442–458, doi:10.1016/j.jseaes.2008.08.002, 2009.

Claoué-Long, J. C., Zhang, Z. C., Ma, G. G., and Du, S.H.: The age of the Permian-Triassic boundary, Earth Planet. Sci. Lett., 105, 182–190, doi:10.1016/0012-821x(91)90129-6, 1991.

Condon, D. J., Schoene, B., McLean, N. M., Bowring, S. A., and Parrish, R. R.: Metrology and traceability of U-Pb isotope dilution geochronology (EARTHTIME Tracer Calibration Part I), Geochim. Cosmochim. Ac., 164, 464–480, doi:10.1016/j.gca.2015.05.026, 2015.

Erwin, D. H.: The End-Permian Mass Extinction, Annu. Rev. Ecol. Syst., 21, 69–91, doi:10.1146/annurev.es.21.110190.000441, 1990.

Erwin, D. H., Bowring, S. A., and Jin, Y.-G.: End-Permian mass-extinctions: a review, in: Catastrophic events and mass extinctions: impacts and beyond, edited by: Koeberl, C. and MacLeod, K. G., Geol. S. Am. S., 356, 353–383, doi:10.1130/0-8137-2356-6.363, 2002.

Faure, M., Lin, W., Chu, Y., and Lepvrier, C.: Triassic tectonics of the southern margin of the South China Block, C. R. Geosci., 348, 5–14, doi:10.1016/j.crte.2015.06.012, 2016.

Feng, Q. L. and Algeo, T. J.: Evolution of oceanic redox conditions during the Permo-Triassic transition: Evidence from deepwater radiolarian facies, Earth-Sci. Rev., 137, 34–51, doi:10.1016/j.earscirev.2013.12.003, 2014.

Feng, Q. L., He, W. H., Gu, S. Z., Meng, Y. Y., Jin, Y. X., and Zhang, F.: Radiolarian evolution during the latest Permian in South China, Global Planet. Change, 55, 177–192, doi:10.1016/j.gloplacha.2006.06.012, 2007.

Feng, Z. Z., Bao, Z.-D., Zheng, X.-J., and Wang, Y.: There was no "Great Bank of Guizhou" in the Early Triassic in Guizhou Province, South China, J. Palaeogeogr., 4, 99–108, doi:10.3724/SP.J.1261.2015.00070, 2015.

Galfetti, T., Bucher, H., Ovtcharova, M., Schaltegger, U., Brayard, A., Brühwiler, T., Goudemand, N., Weissert, H., Hochuli, P. A., Cordey, F., and Guodun, K.: Timing of the Early Triassic carbon cycle perturbations inferred from new U–Pb ages and ammonoid biochronozones, Earth Planet. Sc. Lett., 258, 593–604, doi:10.1016/j.epsl.2007.04.023, 2007.

Galfetti, T., Bucher, H., Martini, R., Hochuli, P. A., Weissert, H., Crasquin-Soleau, S., Brayard, A., Goudemand, N., Brühwiler, T., and Guodun, K.: Evolution of Early Triassic outer platform paleoenvironments in the Nanpanjiang Basin (South China) and their significance for the biotic recovery, Sediment. Geol., 204, 36–60, doi:10.1016/j.sedgeo.2007.12.008, 2008.

Gao, Q., Zhang, N., Xia, W., Feng, Q., Chen, Z.-Q., Zheng, J., Griffin, W. L., O'Reilly, S. Y., Pearson, N. J., Wang, G., Wu, S., Zhong, W., and Sun, X.: Origin of volcanic ash beds across the Permian-Triassic boundary, Daxiakou, South China: Petrology and U-Pb age, trace elements and Hf-isotope composition of zircon, Chem. Geol., 360–361, 41–53, doi:10.1016/j.chemgeo.2013.09.020, 2013.

Golonka, J. and Ford, D.: Pangean (Late Carboniferous-Middle Jurassic) paleoenvironment and lithofacies, Palaeogeogr. Palaeocl., 161, 1–34, doi:10.1016/s0031-0182(00)00115-2, 2000.

Guizhou Bureau of Geology and Mineral Resources: Regional geology of Guizhou Province, scale 1 : 500 000, Geological Memoir, Beijing, 1, 700 pp., 1987 (in Chinese, with English summary).

Haslett, J. and Parnell, A.: A simple monotone process with application to radiocarbon-dated depth chronologies,J. Roy. Stat. Soc. C-App., 57, 399–418, doi:10.1111/j.1467-9876.2008.00623.x, 2008.

He, W. H., Shen, S. Z., Feng, Q. L., and Gu, S. Z.: A Late Changhsingian (Late Permian) deepwater brachiopod fauna from the Talung Formation at the Dongpan section, southern Guangxi, South China, J. Paleontol., 79, 927–938, doi:10.1666/0022-3360(2005)079[0927:ALCLPD]2.0.CO;2, 2005.

He, W. H., Shi, G. R., Feng, Q. L., Campi, M. J., Gu, S. Z., Bu, J. J., Peng, Y. Q., and Meng, Y. Y.: Brachiopod miniaturization and its possible causes during the Permian-Triassic crisis in deep water environments, South China, Palaeogeogr. Palaeocl., 252, 145–163, doi:10.1016/j.palaeo.2006.11.040, 2007.

Hiess, J., Condon, D. J., McLean, N., and Noble, S. R.: ^{238}U/^{235}U Systematics in terrestrial uranium-bearing minerals, Science, 335, 1610–1614, doi:10.1126/science.1215507, 2012.

Hochuli, P. A., Hermann, E., Vigran, J. S., Bucher, H., and Weissert, H.: Rapid demise and recovery of plant ecosystems across the end-Permian extinction event, Global Planet. Change, 74, 144–155, doi:10.1016/j.gloplacha.2010.10.004, 2010.

Huang, C., Tong, J., Hinnov, L., and Chen, Z. Q.: Did the great dying of life take 700 k.y.? Evidence from global astronomical correlation of the Permian-Triassic boundary interval, Geology, 39, 779–782, doi:10.1130/g32126.1, 2011.

Jiang, H., Lai, X., Yan, C., Aldridge, R. J., Wignall, P., and Sun, Y.: Revised conodont zonation and conodont evolution across the Permian-Triassic boundary at the Shangsi section, Guangyuan, Sichuan, South China, Global Planet. Change, 77, 102–115, doi:10.1016/j.gloplacha.2011.04.003, 2011.

Jin, Y. G., Shen, S. Z., Henderson, C. M., Wang, X. D., Wang, W., Wang, Y., Cao, C. Q., and Shang, Q. H.: The Global Stratotype Section and Point (GSSP) for the boundary between the Capitanian and Wuchiapingian stage (Permian), Episodes, 29, 253–262, 2006.

Kuiper, K. F., Deino, A., Hilgen, F. J., Krijgsman, W., Renne, P. R., and Wijbrans, J. R.: Synchronizing Rock Clocks of Earth History, Science, 320, 500–504, doi:10.1126/science.1154339, 2008.

Lehrmann, D. J., Payne, J. L., Felix, S. V., Dillett, P. M., Wang, H., Yu, Y., and Wei, J.: Permian-Triassic Boundary Sections from Shallow-Marine Carbonate Platforms of the Nanpanjiang Basin, South China: Implications for Oceanic Conditions Associated with the End-Permian Extinction and Its Aftermath, Palaios, 18, 138–152, doi:10.1669/0883-1351(2003)18<138:pbsfsc>2.0.co;2, 2003.

Lehrmann, D. J., Pei, D., Enos, P., Ellwood, B. B., Zhang, J., Wei, J., Dillett, P., Koenig, J., Steffen, K., Druke, D., Gross, J., Kessel, B., and Newkirk, T.: Impact of differential tectonic subsidence on isolated carbonate platform evolution: Triassic of the Nanpanjiang basin, south China, Am. Assoc. Petr. Geol. B., 91, 287–320, doi:10.1306/10160606065, 2007.

Lehrmann, D. J., Stepchinski, L., Altiner, D., Orchard, M. J., Montgomery, P., Enos, P., Ellwood, B. B., Bowring, S. A., Ramezani, J., Wang, H., Wei, J., Yu, M., Griffiths, J. D., Minzo, M., Schaall, E. K., Lil, X., Meyerl, K. M., and Payne, J. L.: An integrated biostratigraphy (conodonts and foraminifers) and chronostratigraphy (paleomagnetic reversals, magnetic susceptibility, elemental chemistry, carbon isotopes and geochronology) for the Permian-Upper Triassic strata of Guandao section, Nanpanjiang Basin, south China, J. Asian Earth Sci., 108, 117–135, doi:10.1016/j.jseaes.2015.04.030, 2015.

Li, M., Ogg, J., Zhang, Y., Huang, C., Hinnov, L., Chen, Z.-Q., and Zou, Z.: Astronomical tuning of the end-Permian extinction and the Early Triassic Epoch of South China and Germany, Earth Planet. Sc. Lett., 441, 10–25, doi:10.1016/j.epsl.2016.02.017, 2016.

Luo, G. M., Lai, X. L., Feng, Q. L., Jiang, H. S., Wignall, P., Zhang, K. X., Sun, Y. D., and Wu, J.: End-Permian conodont fauna from Dongpan section: Correlation between the deep- and shallow-water facies. Sci. China Ser. D, 51, 1611–1622, doi:10.1007/s11430-008-0125-1, 2008.

Luo, G. M., Wang, Y., Yang, H., Algeo, T. J., Kump, L. R., Huang, J., and Xie, S. C.: Stepwise and large-magnitude negative shift in $\delta^{13}C_{carb}$ preceded the main marine mass extinction of the Permian-Triassic crisis interval, Palaeogeogr. Palaeocl., 299, 70–82, doi:10.1016/j.palaeo.2010.10.035, 2011.

Mattinson, J. M.: Zircon U-Pb chemical abrasion ("CA-TIMS") method: combined annealing and multi-step partial dissolution analysis for improved precision and accuracy of zircon ages, Chem. Geol., 220, 47–66, doi:10.1016/j.chemgeo.2005.03.011, 2005.

McLean, N. M., Bowring, J. F., and Bowring, S. A.: An algorithm for U-Pb isotope dilution data reduction and uncertainty propagation, Geochem. Geophys. Geosyst., 12, Q0AA18, doi:10.1029/2010gc003478, 2011.

Meng, Y. Y., Zhou, Q., and Li, Y. K.: The characteristics and controlling sedimentary facies and granitoid analysis of the middle part of Pingxing-Dongmeng large fault, Guangxi Geology, 15, 1–4, 2002 (in Chinese).

Mundil, R., Metcalfe, I., Ludwig, K. R., Renne, P. R., Oberli, F., and Nicoll, R. S.: Timing of the Permian-Triassic biotic crisis: Implications from new zircon U/Pb age data (and their limitations), Earth Planet. Sc. Lett., 187, 131–145, doi:10.1016/s0012-821x(01)00274-6, 2001.

Mundil, R., Ludwig, K. R., Metcalfe, I., and Renne, P. R.: Age and Timing of the Permian Mass Extinctions: U/Pb Dating of Closed-System Zircons, Science, 305, 1760–1763, doi:10.1126/science.1101012, 2004.

Ovtcharova, M., Bucher, H., Schaltegger, U., Galfetti, T., Brayard, A., and Guex, J.: New Early to Middle Triassic U-Pb ages from South China: calibration with ammonoid biochronozones and implications for the timing of the Triassic biotic recovery, Earth Planet. Sc. Lett., 243, 463–475, doi:10.1016/j.epsl.2006.01.042, 2006.

Ovtcharova, M., Goudemand, N., Hammer, O., Guodun, K., Cordey, F., Galfetti, T., Schaltegger, U., and Bucher, H.: Developing a strategy for accurate definition of a geological boundary through radio-isotopic and biochronological dating: The Early–Middle Triassic boundary (South China), Earth-Sci. Rev., 146, 65–76, doi:10.1016/j.earscirev.2015.03.006, 2015.

Parnell, A. C., Haslett, J., Allen, J. R. M., Buck, C. E., and Huntley, B.: A flexible approach to assessing synchroneity of past events using Bayesian reconstructions of sedimentation history, Quaternary Sci. Rev., 27, 1872–1885, doi:10.1016/j.quascirev.2008.07.009, 2008.

Parnell, A. C., Buck, C. E., and Doan, T. K.: A review of statistical chronology models for high-resolution, proxy-based Holocene palaeoenvironmental reconstruction, Quaternary Sci. Rev., 30, 2948–2960, doi:10.1016/j.quascirev.2011.07.024, 2011.

Payne, J. L., Turchyn, A. V., Paytan, A., DePaolo, D. J., Lehrmann, D. J., Yu, M. Y., and Wei, J. Y.: Calcium isotope constraints on the end-Permian mass extinction, P. Natl. Acad. Sci. USA, 107, 8543–8548, doi:10.1073/pnas.0914065107, 2010.

Peng, X. F., Feng, Q. L., Li, Z. B., and Meng, Y. Y.: High-resolution cyclostratigraphy of geochemical records from Permo-Triassic boundary section of Dongpan, southwestern Guangxi, South China, Sci. China Ser. D, 51, 187–193, 2008.

Raup, D. M.: Size of the Permo-Triassic bottleneck and its evolutionary implications, Science, 206, 217–218, doi:10.1126/science.206.4415.217, 1979.

Renne, P. R., Black, M. T., Zichao, Z., Richards, M. A., and Basu, A. R.: Synchrony and causal relations between Permian-Triassic Boundary crises and Siberian flood volcanism, Science, 269, 1413–1416, doi:10.1126/science.269.5229.1413, 1995.

Retallack, G. J. and Jahren, A. H.: Methane release from igneous intrusion of coal during Late Permian extinction events, J. Geol., 116, 1–20, doi:10.1086/524120, 2008.

Samperton, K. M., Schoene, B., Cottle, J. M., Keller, C. B., Crowley, J. L., and Schmitz, M. D.: Magma emplacement, differentiation and cooling in the middle crust: Integrated zircon geochronological-geochemical constraints from the Bergell Intrusion, Central Alps, Chem. Geol., 417, 322–340, doi:10.1016/j.chemgeo.2015.10.024, 2015.

Schoene, B., Crowley, J. L., Condon, D. J., Schmitz, M. D., and Bowring, S. A.: Reassessing the uranium decay constants for geochronology using ID-TIMS U-Pb data, Geochim. Cosmochim. Ac., 70, 426–445, doi:10.1016/j.gca.2005.09.007, 2006.

Shang, Q. H., Vachard, D., and Caridroit, M.: Smaller foraminifera from the Late Changhsingian (Latest Permian) of Southern Guangxi and discussion on the Permian-Triassic boundary, Acta Micropalaeontologica Sinica, 20, 377–388, 2003.

Shen, J., Algeo, T. J., Zhou, L., Feng, Q., Yu, J., and Ellwood, B.: Volcanic perturbations of the marine environment in South China preceding the latest Permian mass extinction and their biotic effects, Geobiology, 10, 82–103, doi:10.1111/j.1472-4669.2011.00306.x, 2012.

Shen, J., Algeo, T. J., Hu, Q., Xu, G. Z., Zhou, L., and Feng, Q. L.: Volcanism in South China during the Late

Permian and its relationship to marine ecosystem and environmental changes, Global Planet. Change, 105, 121–134, doi:10.1016/j.gloplacha.2012.02.011, 2013.

Shen, S. Z., Wang, Y., Henderson, C. M., Cao, C. Q., and Wang, W.: Biostratigraphy and lithofacies of the Permian System in the Laibin-Heshan area of Guangxi, South China, Palaeoworld, 16, 120–139, doi:10.1016/j.palwor.2007.05.005, 2007.

Shen, S. Z., Crowley, J. L., Wang, Y., Bowring, S. A., Erwin, D. H., Sadler, P. M., Cao, C. Q., Rothman, D. H., Henderson, C. M., Ramezani, J., Zhang, H., Shen, Y., Wang, X. D., Wang, W., Mu, L., Li, W. Z., Tang, Y. G., Liu, X. L., Liu, L. J., Zeng, Y., Jiang, Y. F., and Jin, Y. G.: Calibrating the end-Permian mass extinction, Science, 334, 1367–1372, doi:10.1126/science.1213454, 2011.

Shen, S. Z., Cao, C. Q., Zhang, H., Bowring, S. A., Henderson, C. M., Payne, J. L., Davydov, V. I., Chen, B., Yuan, D. X., Zhang, Y. C., Wang, W., and Zheng, Q. F.: High-resolution $\delta^{13}C_{carb}$ chemostratigraphy from latest Guadalupian through earliest Triassic in South China and Iran, Earth Planet. Sc. Lett., 375, 156–165, doi:10.1016/j.epsl.2013.05.020, 2013.

Stanley, S. M. and Yang, X.: A double mass extinction at the end of the Paleozoic era, Science, 266, 1340–1344, doi:10.1126/science.266.5189.1340, 1994.

Svensen, H., Planke, S., Polozov, A. G., Schmidbauer, N., Corfu, F., Podladchikov, Y. Y., and Jamtveit, B.: Siberian gas venting and the end-Permian environmental crisis, Earth Planet. Sc. Lett., 277, 490–500, doi:10.1016/j.epsl.2008.11.015, 2009.

Van Valen, L.: A resetting of Phanerozoic community evolution, Nature, 307, 50–52, doi:10.1038/307050a0, 1984.

Wang, Y. and Jin, Y.: Permian palaeogeographic evolution of the Jiangnan Basin, South China, Palaeogeogr. Palaeocl., 160, 35–44, doi:10.1016/s0031-0182(00)00043-2, 2000.

Winguth, C. and Winguth, A. M. E.: Simulating Permian-Triassic oceanic anoxia distribution: implications for species extinction and recovery, Geology, 40, 127–130, doi:10.1130/g32453.1, 2012.

Wu, H., Zhang, S., Hinnov, L. A., Jiang, G., Feng, Q., Li, H., and Yang, T.: Time-calibrated Milankovitch cycles for the late Permian, Nat. Commun., 4, 2452, doi:10.1038/ncomms3452, 2013.

Wu, J., Feng, Q. L., Gui, B. W., and Liu, G. C.: Some new radiolarian species and genus from Upper Permian in Guangxi Province, South China, J. Paleontol., 84, 879–894, doi:10.1666/09-057.1, 2010.

Xia, W. C., Zhang, N., Wang, G. Q., and Kakuwa, Y.: Pelagic radiolarian and conodont biozonation in the Permo-Triassic boundary interval and correlation to the Meishan GSSP, Micropaleontology, 50, 27–44, doi:10.1661/0026-2803(2004)050[0027:pracbi]2.0.co;2, 2004.

Yin, H. F.: Bivalves near the Permian-Triassic boundary in South China, J. Paleontol., 59, 572–600, 1985.

Yin, H. F., Zhang, K. X., Tong, J. N., Yang, Z. Y., and Wu, S. B.: The global stratotype section and point (GSSP) of the Permian-Triassic boundary, Episodes, 24, 102–114, 2001.

Yin, H. F., Feng, Q. L., Lai, X. L., Baud, A., and Tong, J. N.: The protracted Permo-Triassic crisis and multi-episode extinction around the Permian-Triassic boundary, Global Planet. Change, 55, 1–20, doi:10.1016/j.gloplacha.2006.06.005, 2007.

Yin, H. F., Jiang, H. S., Xia, W. C. Feng, Q., Zhang, N., and Shen, J.: The end-Permian regression in South China and its implication on mass extinction, Earth-Sci. Rev., 137, 19–33, doi:10.1016/j.earscirev.2013.06.003, 2014.

Yuan, A., Crasquin-Soleau, S., Feng, Q. L., and Gu, S. Z.: Latest Permian deep-water ostracods from southwestern Guangxi, South China, J. Micropalaeontol., 26, 169–191, doi:10.1144/jm.26.2.169, 2007.

Yuan, D., Shen, S., Henderson, C. M., Chen, J., Zhang, H., and Feng, H.: Revised conodont-based integrated high-resolution timescale for the Changhsingian Stage and end-Permian extinction interval at the Meishan sections, South China, Lithos, 204, 220–245, doi:10.1016/j.lithos.2014.03.026, 2015.

Zhang, F., Feng, Q. L., He, W. H., Meng, Y. Y., and Gu, S. Z.: Multidisciplinary stratigraphy across the Permian-Triassic boundary in deep-water environment of Dongpan section, south China, Norw. J. Geol., 86, 125–131, 2006.

Zhao, J. K., Liang, X. L., and Zheng, Z. G.: Late Permian Cephalopods in South China, Science Press, Beijing, China, 1978 (in Chinese).

Ziegler, A. M., Hulver, M. L., and Rowley, D. B.: Permian World Topography and Climate, in: Late glacial and postglacial environmental changes: Quaternary, Carboniferous-Permian, and Proterozoic, edited by: Martini, I. P., Oxford University Press, New York, USA, 343 pp., 1997.